

# An exact solution for a steady, flow-line marine ice sheet

Ed Bueler

*Department of Mathematics and Statistics and Geophysical Institute, University of Alaska Fairbanks, USA*  
*E-mail: elbueler@alaska.edu*

**ABSTRACT.** G. Böðvarsson’s 1955 plug flow solution for an Icelandic glacier problem is shown to be an exact solution to the steady form of the simultaneous stress balance and mass continuity equations widely-used in numerical models of marine ice sheets. The solution, which has parabolic ice thickness and constant vertically-integrated longitudinal stress, solves the steady shallow shelf approximation with linear sliding on a flat bed. It has elevation-dependent surface mass balance and, in the interpretation given here, a contrived location-dependent ice hardness distribution. By connecting Böðvarsson’s solution to the van der Veen (1983) solution for floating ice, we construct an exact solution to the “rapid-sliding” marine ice sheet problem, continuously across the grounding line. We exploit this exact solution to examine the accuracy of two numerical methods, one grid-free and the other based on a fixed, equally-spaced grid.

## INTRODUCTION

Early theoretical glaciology created two fundamentally-different parabolic profiles as the shapes of steady flow-line ice sheets lying on flat beds, as in Figure 1. One was the profile of an ice sheet with perfect-plasticity (Orowan, 1949; Nye, 1952) and the other the profile for a sliding “plug” flow investigated by Böðvarsson (1955). These global views of free surface flows in glaciology focus on different aspects of the problem and they come to rather different conclusions. Up to scaling, one is of the form  $x = 1 - y^2$  (Orowan-Nye) and the other is of the form  $y = 1 - x^2$  (Böðvarsson). The former perfect-plasticity solution has a central peak at the highest point of the ice sheet, and a margin with unbounded surface gradient. The latter plug flow solution has a smooth dome and a finite-slope, wedge-shaped margin.

This paper shows how to combine Böðvarsson’s solution with the well-known exact solution for an ice shelf (van der Veen, 1983, 2013) to generate an exact solution for a flowline, steady marine ice sheet. It is shown in Figure 2. This exact solution simultaneously solves the steady mass continuity equation and the so-called shallow shelf approximation (“SSA”; Weis and others, 1999) stress balance. It is an exact solution in the rapidly-sliding marine ice sheet case (Schoof, 2007), the model addressed by the MIS-MIP intercomparison (Pattyn and others, 2012). After presenting the model equations and constructing the exact solution in the next two sections, we examine errors made by two different numerical methods. We observe, through linearization of the equations around the exact solution, that the grounding line generates a strong “stiffness” constraint.

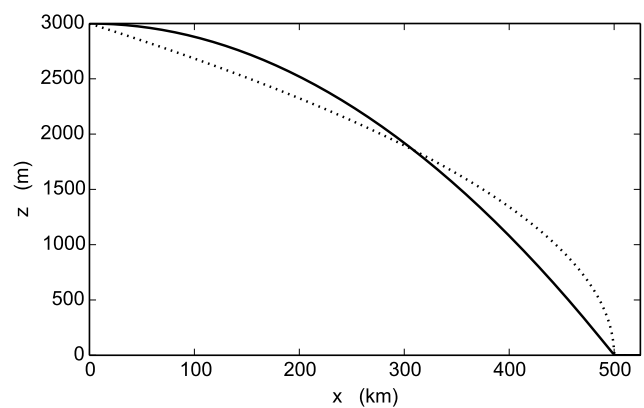


**Fig. 1.** The parabolas by Orowan and Nye (1949, 1952; dotted) and by Böðvarsson (1955; solid) for steady, flowline ice sheets on flat beds. A dome thickness of  $H_0 = 3000$  m and a length of  $L_0 = 500$  km are chosen for concreteness.

## CONTINUUM MODEL

### Model equations

Our model equations describe the steady-state, flat bed form of the flowline, rapid-sliding model of Schoof (2007; equations (2.1)–(2.5)), but we restrict to the linear sliding case. The primary unknowns in these equations are the ice thickness  $H(x)$ , velocity  $u(x)$ , and vertically-integrated longitudinal stress  $T(x)$  (Schoof, 2006), where  $x$  is the flowline distance. Using notation from Table 1, the equations are

$$(uH)_x - M = 0, \quad (1)$$

$$T_x - \beta u - \rho g H h_x = 0, \quad (2)$$

$$T = 2BH|u_x|^{\frac{1}{n}-1}u_x. \quad (3)$$

Here the subscript  $x$  denotes the derivative and

$$h = \begin{cases} H + b, & \rho H \geq \rho_w(z_o - b) \\ \omega H + z_o, & \rho H < \rho_w(z_o - b) \end{cases}, \quad (4)$$

$$\beta = \begin{cases} k\rho g H, & \rho H \geq \rho_w(z_o - b) \\ 0, & \rho H < \rho_w(z_o - b) \end{cases}, \quad (5)$$

are the surface elevation and sliding coefficient, respectively.

Equations (1)–(5) apply on an interval  $0 < x < x_c$  where  $x_c$  is the floating calving-front. The grounded ice rests on flat bedrock at elevation  $b$ , a constant in this context. Note that  $M(x)$  combines the surface and basal mass balance; it is the accumulation/ablation rate function for a vertically-integrated moving layer. The coefficient  $B(x)$  in (3) is called the ice “hardness.” In grounded ice the basal shear stress satisfies  $\tau_b = -\beta u$  (MacAyeal, 1989), and we have scaled the coefficient with the ice overburden pressure so that  $\beta = k\rho g H$  (Böðvarsson, 1955). The “Archimedean factor”  $\omega = 1 - \rho/\rho_w$  relates surface elevation to thickness in floating ice. Note  $z_o$  is the elevation of the ocean surface.

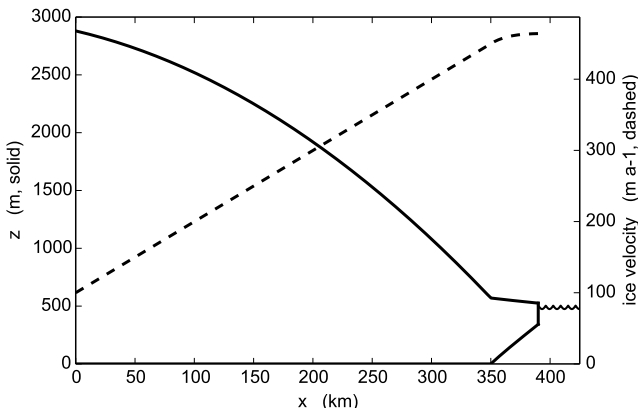


**Fig. 2.** The geometry (solid) and velocity (dashed) of an exact solution of the simultaneous steady mass continuity and SSA stress balance equations for a marine ice sheet. The solution is Böðvarsson’s when grounded and van der Veen’s when floating.

Equations (1) and (2) are the mass-continuity and SSA stress balance equations, respectively, while (3) defines  $T$ . Equation (4) says that the ice surface  $z = h$  is at elevation  $H + b$  when the ice is grounded, and otherwise the ice surface  $z = h$  is found from the Archimedean principle. Likewise equation (5) gives the scaled form of the basal shear stress for grounded ice; it is zero for floating ice. We must solve for the location of the grounding line  $x = x_g$ , but at it we know  $\rho H(x_g) = \rho_w(z_o - b)$ .

For the exact and numerical solutions in this paper, equations (1)–(5) are augmented by boundary

conditions:

$$u(0) = u_a > 0, \quad H(0) = H_a > 0, \quad (6)$$

$$T(x_c) = \frac{1}{2}\omega\rho g H(x_c)^2, \quad (7)$$

$$H, u, T \quad \text{continuous at } x = x_g. \quad (8)$$

Here  $x = 0$  is an upstream location where Dirichlet boundary conditions are applied (equation (6)), while at the calving front  $x = x_c$  we have the standard hydrostatic pressure “imbalance” condition (7) (Schoof, 2007). Facts (8) at  $x_g$  may be regarded as a regularity requirement, and not strictly a boundary condition; see below.

### On well-posedness and the grounding line

Given data  $B(x)$ ,  $b$ ,  $k > 0$ ,  $M(x)$ ,  $x_c > 0$ ,  $z_o$ , along with physical constants  $g, n, \rho, \rho_w$ , we expect the problem consisting of equations (1)–(8) to be well-posed. To our knowledge this has not been proved, nor do we attempt to prove it. It is, however, worth considering the smoothness (regularity) of the solution to (1)–(7), including what hypotheses would lead to satisfying (8) at the free (unknown) location  $x_g$  in the interior of the domain.

Indeed, suppose that, for physical reasons, the mass balance  $M(x)$  and ice hardness  $B(x)$  are bounded, and further that  $B(x)$  is bounded below by a positive constant. From integrating  $M$ , equation (1) implies that the flux  $q = uH$  is absolutely-continuous and thus bounded. If there is a positive lower bound on thickness  $H$ , then we can conclude that the magnitude of  $u$  is bounded because  $u = q/H$ . If the magnitude of the driving stress  $-\rho g H h_x$  is bounded then equation (2) implies  $T$  is absolutely-continuous. By equation (3) this implies  $u$  has a bounded and integrable derivative, and thus that  $u$  is also absolutely-continuous. From these facts we could then return to the flux and write  $H = q/u$  which shows  $H$  is absolutely-continuous away from locations where  $u = 0$  (e.g. divides). In summary, assuming (i) that an integrable solution  $(H, u, T)$  to (1)–(7) exists, (ii) that the functions  $M, B$  are bounded and integrable, (iii) that  $B$  is bounded below by a positive constant, (iv) that a positive lower bound on thickness exists, and (v) that an upper bound on the magnitude of the driving stress exists, then we can regard conditions (8), giving continuity at the grounding line, as properties of the solution instead of as part of the “imposed” problem statement.

## EXACT SOLUTION

### Böðvarsson’s parabola

Böðvarsson (1955) built, based on minimal existing literature, a rigorous theory of the flow of glaciers

**Table 1.** Notation and SI units. Values of physical constants.

Symbol	Description	Units
$B$	ice hardness; $= A^{-1/n}$	$\text{Pa s}^{1/3}$
$b$	bedrock elevation	m
$\beta$	sliding coefficient	$\text{Pa s m}^{-1}$
$g$	acceleration of gravity	$9.81 \text{ m s}^{-2}$
$H$	ice thickness	m
$h$	ice surface elevation	m
$k$	pressure-scaled sliding coefficient	$\text{s m}^{-1}$
$M$	mass balance	$\text{m s}^{-1}$
$n$	Glen exponent in ice flow law	3
$\rho$	density of ice	$910 \text{ kg m}^{-3}$
$\rho_w$	density of sea water	$1028 \text{ kg m}^{-3}$
$T$	$z$ -integrated longitudinal stress	Pa m
$\tau_b$	basal shear stress applied to ice	Pa
$u$	horizontal velocity	$\text{m s}^{-1}$
$(x, z)$	flow-line cartesian coordinates	m
$x_g$	grounding line	m
$x_c$	calving front	m
$z_o$	ocean surface elevation	m
$\omega$	Archimedean factor; $= 1 - \rho/\rho_w$	0.115

and ice sheets. His test case was Brúarjökull, a glacier on the northern margin of Vatnajökull in Iceland. It flows over a smooth bed for 20 km, from a location where its thickness is 600 m, to a zero thickness margin. This glacier is entirely grounded. He shows that a good fit to measured surface elevations can be made using his model.

He initially states an equation for the ice sheet surface elevation which has both vertical-plane shear and longitudinal stress within the ice. However, he says this equation “is quite tedious and very difficult to handle especially because of the [shear] term in the parentheses. It is therefore fortunate that [the shear] term appears to be small compared to the [basal sliding] term.” Then he drops the shear term and writes an equation in which driving stress is balanced entirely by sliding resistance. He solves and analyzes this plug flow model, which we now detail.

As is perhaps best-known about Bððvarsson’s work, he chooses the surface mass balance to be

$$M = a(H - H_{\text{ela}}) \quad (9)$$

for a mass balance gradient  $a > 0$  and equilibrium-line altitude  $H_{\text{ela}}$ . For basal resistance he chooses a coefficient which scales with the overburden pressure, so that the basal shear stress is

$$\tau_b = -\beta u = -k\rho g H u \quad (10)$$

He then writes the ice flux as  $uH = -(H/k)H_x$ , or equivalently the ice velocity as

$$u = -\frac{1}{k}H_x. \quad (11)$$

We will see that equation (11) can be derived from equations (2) and (10) in the special case where  $T_x = 0$  and the bed is flat.

Combining equations (9) and (11) with mass continuity (1) yields equation (17) in (Bððvarsson, 1955), namely

$$a(H - H_{\text{ela}}) + (k^{-1}HH_x)_x = 0. \quad (12)$$

His thickness solution to this equation is (Bodvarðsson, 1955, equations (18) and (23))

$$H(x) = H_0(1 - (x/L_0)^2) \quad (13)$$

where  $H_0 = 1.5H_{\text{ela}}$  and  $akL_0^2 = 9H_{\text{ela}}$  (Bodvarðsson, 1955, equation (24)).

Despite its simplicity, equation (13) is an exact solution to equation (12), with boundary condition  $H(0) = H_0$ , as the reader may verify. Formula (13) defines the solid parabola shown in Figure 1. Bððvarsson does not offer a reason why there should be such a simple quadratic solution to (13). In fact, his solution seems to be a new result for a narrow class of nonlinear second-order ODEs; see Appendix A.

He explicitly considers solution (13) as solving a free boundary problem, in the sense that the single boundary condition  $H(0) = H_0$  applied to the equation (12) determines the quadratic solution (13); see Appendix A. Solving (12) with this single boundary condition generates a location  $x = L_0$  where both the flux and the thickness are zero.

Bððvarsson (1955) was apparently first cited by Weertman (1961), who decided that his sliding, plug-flow physics should be replaced by a shear deformation model more like the shallow ice approximation. This replacement seems to have influenced readers from then on. Nonetheless Bððvarsson had a particular “sliding law” in mind, namely equation (10), in which the sliding coefficient scales with overburden pressure. The modern reader may protest that  $\beta$  should instead be a function of, perhaps even proportional to, effective pressure  $N = \rho g H - P$  where  $P$  is the subglacial water pressure. However, it is not unreasonable to suppose that basal water pressure also scales with (i.e. is roughly a fixed fraction of) overburden pressure. In that case we have equations  $\beta = cN$ ,  $N = \rho g H - P$ , and  $P = \lambda \rho g H$  which combine to  $\beta = c(1 - \lambda)\rho g H$ . In other words, as in Bððvarsson’s model we have  $\beta = k\rho g H$  with  $k = c(1 - \lambda)$ .

The surface balance parameterization (9) reappears in Weertman (1961), among many other places. It realistically parameterizes a potential climatic instability, which was Bððvarsson’s, Weertman’s, and most readers’, major interest. We are, however, interested now in Bððvarsson’s solution to the ice flow equations themselves.

### An SSA re-interpretation

We have claimed that (13) exactly solves a combination of the steady flow-line mass-continuity equation (1) and the SSA stress balance equation (2). In fact, suppose we look for solutions of (1) and (2) with constant vertically-integrated longitudinal stress,  $T_x = 0$ . In that case equation (2) and the scaling (10) implies B  dvarsson’s formula for the velocity, namely equation (11). Furthermore, equations (1) and (9) then give B  dvarsson’s main equation (12). That is, if (i)  $T_x = 0$ , (ii) sliding resistance is linear and scales with overburden pressure, and (iii) mass balance is proportional to elevation above the equilibrium line, then we can recover a simple parabolic profile for  $H(x)$ , namely equation (13) which is a solution to (12).

But what does the condition “ $T_x = 0$ ” imply as a relation among the modeled quantities? Given a thickness profile  $H(x)$  and a strain rate profile  $u_x(x)$ , we may interpret  $T_x = 0$  as a statement of *variable ice hardness*  $B(x)$ . Some such hardness variation is physical, for example in numerical models which use the SSA in a temperature-dependent way (Bueler and Brown, 2009), so that assuming  $x$ -dependent hardness requires no conceptual extensions in the marine ice sheet modeling context. Numerical models which might use for verification the exact solution we are building will often require no modifications to incorporate variable hardness. By contrast, the variable hardness  $B(x)$  used here allows us to “manufacture” an exact solution (Bueler and others, 2005) from the assumption that  $T = T_0$  is constant. That assumption used in equation (3) yields a formula for ice hardness,

$$B(x) = \frac{T_0}{2H|u_x|^{(1/n)-1}u_x}. \quad (14)$$

This formula determines ice hardness in our context because (13) defines  $H(x)$ , so then (11) defines  $u(x)$ , and then we compute  $u_x$  and use (14).

### Extending the exact solution to floating ice

The value  $T_0$  in (14) can be set by a downstream stress condition, just as it is in many models for flowline ice shelves (e.g. Pattyn and others, 2012; Schoof, 2007). Two well-known observations are relevant: (i) For floating ice with  $\beta = 0$ , equations (1)–(7) also have a known exact solution, specifically in the case where the mass balance  $M$  and the ice hardness  $B$  are constant (van der Veen, 1983, 2013). (ii) The vertically-integrated longitudinal stress  $T$  in a flowline ice shelf (i.e. one without lateral stresses) satisfies equation (7) at each location  $x$  in the shelf, that is,  $T(x) = \frac{1}{2}\omega\rho gH(x)^2$ , because this is a first integral of equation (2) if  $\beta = 0$ .

Based on these observations we can construct a marine ice sheet exact solution by extending B  dvarsson’s grounded solution to the floating ice. First taking  $b = 0$  as the flat bed elevation, we suppose the ocean has surface elevation  $z_o > 0$ , thus determining the grounding-line thickness  $H(x_g) = (\rho_w/\rho)z_o$ . Then from B  dvarsson’s thickness solution (13) we can determine  $x_g$ . At  $x_g$ , from (11) and (13), we know  $u(x_g)$  as well. For  $x_g \leq x \leq x_c$ , the floating ice shelf, we then set  $M(x) = M(x_g)$  as constant from the formula (9), thus making  $M(x)$  continuous across the grounding line, while at the same time allowing us to use van der Veen’s construction (which is based on constant mass balance). The equation  $T(x) = \frac{1}{2}\omega\rho gH(x)^2$  determines  $T_o = T(x_g)$  for use in equation (14), which determines  $B(x_g)$  in particular, and so then we set  $B(x) = B(x_g)$  for  $x_g \leq x \leq x_c$ , a constant needed in van der Veen’s construction.

The results of the above choices are the following formulae for an exact marine ice sheet satisfying our steady model equations (1)–(8). The velocity comes from combining the B  dvarsson (1955) and van der Veen (1983) results,

$$u(x) = \begin{cases} \frac{2H_0}{kL_0^2}(x + x_a), & 0 \leq x \leq x_g, \\ u_s(x), & x_g \leq x \leq x_c. \end{cases} \quad (15)$$

where  $u_s(x)$  is defined by

$$u_s(x)^{n+1} = u(x_g)^{n+1} + \frac{C_s}{M(x_g)}(Q_s(x)^{n+1} - Q_g^{n+1}), \quad (16)$$

$C_s = (\rho g \omega / (4B(x_g)))^n$ ,  $Q_g = u(x_g)H(x_g)$ , and  $Q_s(x) = Q_g + M(x_g)(x - x_g)$ . Similarly the thickness is:

$$H(x) = \begin{cases} H_0 \left(1 - \left(\frac{x+x_a}{L_0}\right)^2\right), & 0 \leq x \leq x_g, \\ \frac{Q_s(x)}{u_s(x)}, & x_g \leq x \leq x_c. \end{cases} \quad (17)$$

Formulas (15) and (17) define the continuous functions which are shown in Figure 2, using the specific values in Table 2.

From the thickness  $H(x)$  and the velocity  $u(x)$  we can find continuous functions  $M(x)$  and  $B(x)$  for the full flowline by using equations (9) and (14). These functions are shown in Figure 3. Then we can use equation (3) to find  $T(x)$ ; this is shown in Figure 4. In Figure 4 we also show the sliding coefficient  $\beta(x)$ , which drops to zero discontinuously at  $x_g$ . Finally Figure 5 shows a detail of the grounding line and floating ice in the exact solution.

The floating ice shelf is a relatively short 40 km; see Figures 2 and 5. To explain, note that the equilibrium line  $H_{\text{ela}}$  in B  dvarsson’s (1955) solution is high on the ice sheet because of its relation to the upstream ice thickness in the construction of the

**Table 2.** Specific values used in (above line) or determined by (below line) the equations which define the exact solution shown in Figures 2–5. Note “g.l.” = grounding line and “c.f.” = calving front.

Symbol	Description	Units
$a$	mass balance gradient	$0.003 \text{ a}^{-1}$
$b$	bedrock elevation	0 m
$H_0$	thickness used in (13)	3000 m
$H_{\text{ela}}$	equilibrium line altitude	2000 m
$k$	scaled sliding coefficient	$757.366 \text{ s m}^{-1}$
$L_0$	length used in (13)	500 km
$x_a$	offset	100 km
$z_o$	ocean surface elevation	504.572 m
$H(0)$	thickness at $x = 0$	2880 m
$u(0)$	ice velocity at $x = 0$	$100 \text{ m a}^{-1}$
<hr/>		
$x_g$	location of g.l.	350 km
$B(x_g)$	ice hardness at g.l.	$4.614 \times 10^8 \text{ Pa s}^{1/3}$
$H(x_g)$	thickness at g.l.	570 m
$M(x_g)$	mass balance at g.l.	$-4.290 \text{ m a}^{-1}$
$T(x_g)$	stress at g.l.	$1.665 \times 10^8 \text{ Pa m}$
$u(x_g)$	ice velocity at g.l.	$450 \text{ m a}^{-1}$
$x_c$	location of c.f.	390 km
$H(x_c)$	thickness at c.f.	182.938 m
$T(x_c)$	stress at c.f.	$0.171 \times 10^8 \text{ Pa m}$
$u(x_c)$	ice velocity at c.f.	$464.092 \text{ m a}^{-1}$

exact solution (i.e.  $H_{\text{ela}} = (2/3)H_0$ ). This in turn implies  $M(x_g)$  is quite negative (equation (9); see Figure 3). Because van der Veen’s (1983) solution uses constant mass balance, and because we want continuity for  $M(x)$ , we therefore have an ice shelf experiencing rapid melting. The location of the calving front  $x_c$  must, of course, be put upstream of the location where the ice has melted away. As a result of these same factors we also see a rapid decline in the stress  $T(x)$  from its constant grounded value to its small value at  $x_c$  (Figure 4 and Table 2). Though the ice shelf shown here is very wedge-like, the thickness  $H(x)$  for floating ice comes from formula (17), and it is not a linear function because  $u_s(x)$  is not constant on the shelf.

## NUMERICAL RESULTS

### Verification of a grid-free “shooting” numerical method

In our steady flowline case the model equations form a two-point boundary value problem (BVP) for ordinary differential equations (ODEs). Specifically, the three first-order ODEs (1)–(3) are subject to two boundary conditions (6) at  $x = 0$  and one at  $x = x_c$ , the calving-front stress condition (7).

A nonlinear “shooting” method (Press and others, 1992, section 17.1) applies to this problem. We use the correct values for  $u(0)$  and  $H(0)$  from (6) and guess an additional value  $T_0$  for  $T(0)$ . Then we use

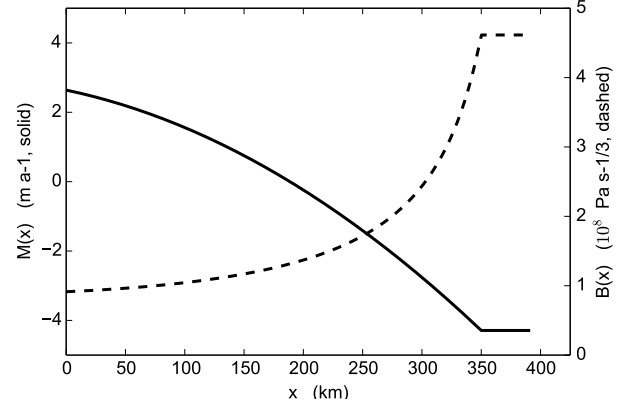


**Fig. 3.** The mass balance  $M(x)$  (solid) and ice hardness  $B(x)$  (dashed) of the exact solution.

a numerical ODE initial value problem (IVP) solver to compute a solution  $(\tilde{u}(x), \tilde{H}(x), \tilde{T}(x))$  from  $x = 0$  to  $x = x_c$ . The failure of the ODE IVP solution to satisfy boundary condition (7) is a measure of the wrongness of  $T_0$ . In fact, based on (7) we define the function

$$F(T_0) = \tilde{T}(x_c) - \frac{1}{2}\omega\rho g\tilde{H}(x_c)^2 \quad (18)$$

and then we can apply a numerical method to find the solution (root)  $\hat{T}_0$  to the problem  $F(T_0) = 0$ . This root gives us complete initial conditions so that the ODE IVP solution also solves the two-point BVP (1)–(7).

A robust root-finding method is bisection (Press and others, 1992, section 9.1). It is guaranteed to converge if  $F$  is continuous and if an initial bracket is given (easy to find in this case). Regarding faster root-finding methods than bisection, such as Newton’s method, we observe that  $F'$  may not exist because of the low regularity of the solution at the interior point  $x = x_g$ . However, by using our exact solution we will see clear evidence that the bisection iteration succeeds in finding the root  $\hat{T}_0$  to many digits despite the uncertain smoothness of  $F$ .

This “shooting” method has the advantage that the advanced stepsize control mechanism of an ODE IVP solver determines the spatial grid points, so as to solve the ODEs to a desired tolerance. Thereby we avoid *a priori* choice of the grid, and in this sense the method is grid-free. In this case we use LSODA from the ODEPACK collection (Hindmarsh, 1983) because it both automatically adjusts stepsize to achieve desired tolerance and because it automatically switches method when stiffness (Press and others, 1992, section 16.6) is detected.

We now apply this grid-free procedure to the same problem for which we have the exact solution (equa-

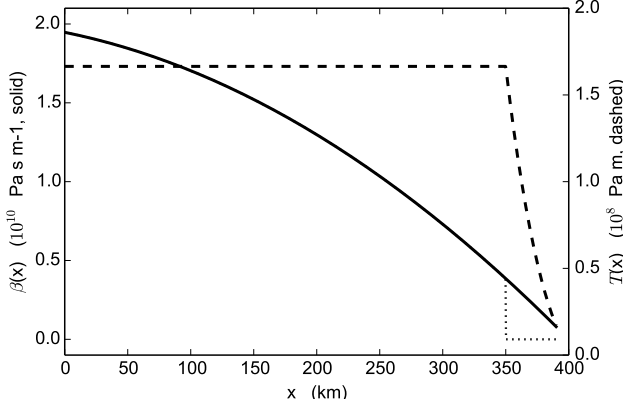


**Fig. 4.** The sliding coefficient  $\beta(x)$  (solid) and the vertically-integrated longitudinal stress  $T(x)$  (dashed) for the exact solution. The solid curve shows  $\beta = k\rho gH$  on both sides of the grounding line. The actual basal resistance experienced by the shelf drops to zero at the grounding line (dotted).

tions (15)–(17)). Using relative tolerance  $10^{-12}$  and absolute tolerance  $10^{-14}$  for LSODA we get the results in Figure 6. We have shown the error in two runs, one in which we have used the exactly-correct initial value  $T_0$  (“cheating”) and one in which we start with a large initial bracket on  $T_0$  and converge on the correct calving-front boundary condition through shooting and bisection (“realistic”). In the “cheating” runs we see that the numerical error just from solving the ODE, i.e. independent of errors in boundary conditions, is quite small, perhaps the 10th or 11th digit for  $H$  and  $u$ . The much larger error seen in the “realistic” case suggests, however, that  $F$  in (18) is significantly irregular. Apparently matching the calving-front boundary condition by numerical shooting from upstream causes the loss of 4 or 5 digits of accuracy. Nonetheless, in this “realistic” case our numerical method achieves 6 or 7 digit accuracy over the whole domain, including in the immediate vicinity of the grounding line. Note that though the peak inaccuracy is near the grounding line, that error is only modestly larger than errors elsewhere.

The ODE solver also detects the grounding line as a point of transition to shorter (spatial) steps, as seen in Figure 7. More significantly, however, the grounded ice requires a stiff method while the floating ice allows a nonstiff one, according to the automatic switch mechanism in LSODA. Note that high accuracy (e.g. 6 or 7 digits) is achieved in the “realistic” case despite rather large grid spacing in the grounded ice, with large portions at 5–10 km spacing. The spacing drops to a minimum of 100 m just downstream of the grounding line at  $x_g = 350$  km.

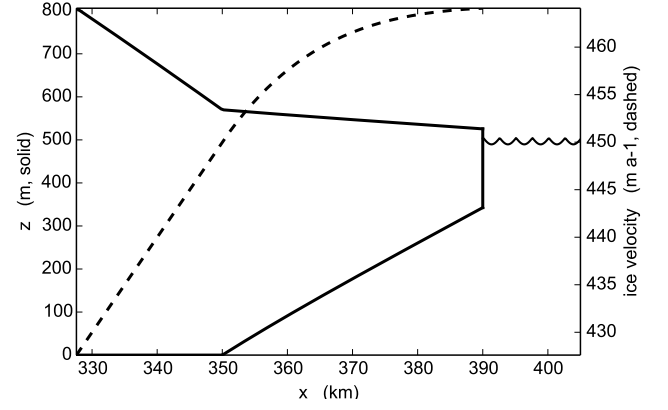


**Fig. 5.** Detail of Figure 2, showing the floating ice shelf geometry and velocity.

In all numerical tests we have treated  $M(x)$  as a predetermined field (i.e. the one shown in Figure 3). This removes the climatically-important elevation–accumulation feedback, and the associated instability, of interest to Böðvarsson (1955) and others. This feedback can, however, be restored by using equation (9) to determine  $M$  from  $H$ .

### Linearization around the exact solution

The above numerical evidence shows that a distinct change in stiffness occurs at the grounding line. To analyze this we linearize the model equations around the exact solution. Denote the exact solution  $(u_0, H_0, T_0)$  and consider a small perturbation  $u = \hat{u} + \epsilon \tilde{u}$ ,  $H = \hat{H} + \epsilon \tilde{H}$ , and  $T = \hat{T} + \epsilon \tilde{T}$ . Denote the column vector of perturbations by  $\mathbf{w} = [\tilde{u}, \tilde{H}, \tilde{T}]^T$ . Assuming  $u_x > 0$ , equations (1)–(3) imply that, to first order in  $\epsilon$ , the perturbation solves this linear ODE system in grounded ice,

$$\begin{bmatrix} \frac{2}{n} B \hat{H} (\hat{u}_x)^q & 0 & 0 \\ \hat{H} & \hat{u} & 0 \\ 0 & -\rho g \hat{H} & 1 \end{bmatrix} \mathbf{w}_x = \begin{bmatrix} 0 & -2B(\hat{u}_x)^{1/n} & 1 \\ -\hat{H}_x & -\hat{u}_x & 0 \\ -k\rho g \hat{H} & -k\rho g \hat{u} + \rho g \hat{H}_x & 0 \end{bmatrix} \mathbf{w} \quad (19)$$

where  $q = \frac{1}{n} - 1$ . In floating ice only the last rows differ from (19):

$$\begin{bmatrix} \dots \\ 0 & -\omega \rho g \hat{H} & 1 \end{bmatrix} \mathbf{w}_x = \begin{bmatrix} \dots \\ 0 & \omega \rho g \hat{H}_x & 0 \end{bmatrix} \mathbf{w} \quad (20)$$

If we define  $L(x)$  and  $R(x)$  to be the left- and right-side matrices in (19) and (20) then  $\mathbf{w}$  solves

$$\mathbf{w}_x = A(x) \mathbf{w} \quad (21)$$

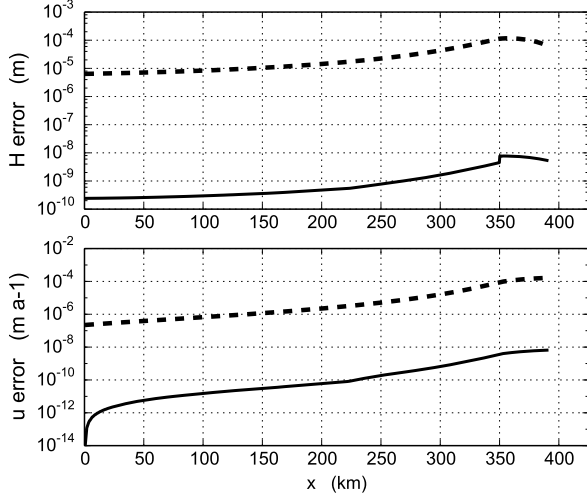


**Fig. 6.** Pointwise error in thickness (upper panel) and in velocity (lower panel) from an adaptive numerical ODE scheme. Both the “cheating” case (solid), where we use the exactly-correct initial value for  $T$ , and the “realistic” case (dashed), where the shooting method converges on the correct initial value for  $T$  by the bisection method, are shown.

along its whole length, where  $A(x) = L(x)^{-1}R(x)$ . Note that we have chosen  $L(x)$  to be lower triangular. The inverse of  $L(x)$  exists, and is easy to compute, because its diagonal entries are nonzero.

The linear ODE system (21) is stiff if there is a large ratio of magnitudes in the eigenvalues of  $A(x)$  (Press and others, 1992). Because the entries and eigenvalues of  $A(x)$  are exactly computable using the exact solution values ( $\hat{u}(x)$ ,  $\hat{H}(x)$ ,  $\hat{T}(x)$ ), we can plot, along the whole length of the flowline, the  $x$ -dependent “stiffness ratio” for  $A(x)$ , namely the ratio of absolute values of the real parts of the largest and smallest eigenvalues of  $A(x)$ . See Figure 8. This ratio is small in the nonstiff case, and it is independent of the direction of integration (i.e. upstream versus downstream). The computed ratio is by no means the last word on quantifying stiffness, which turns out to be difficult generally (e.g. Higham and Trefethen, 1993).

We believe that the strong stiffness contrast at the grounding line is significant in explaining large near-grounding-line errors made by gridded numerical methods (Gladstone and others, 2010; Pattyn and others, 2012). The stiffness ratio drops by a factor of almost ten at the grounding line, though it is largest in the interior part of the grounded ice. It is possible that models of modified effective pressure near the grounding line (Leguy and others, 2014), in sliding laws that are parameterized by effective pres-

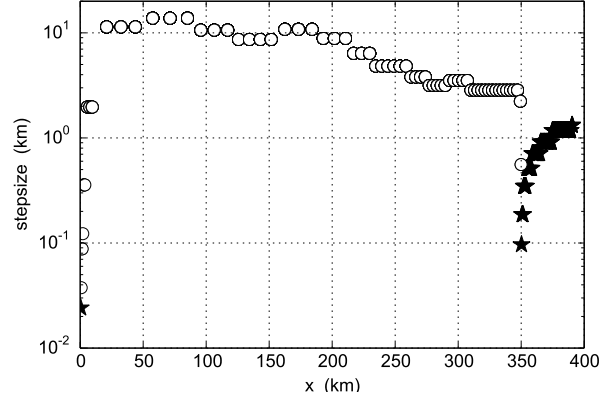


**Fig. 7.** The adaptive numerical ODE scheme in the “realistic” case makes steps of 1 km to 10 km in grounded ice, but at the grounding line  $x_g = 350$  km the step size is reduced to a few hundred meters. The adaptive mechanism automatically switches from a stiff method where grounded (circles) to a non-stiff method where floating (stars).

sure (Schoof, 2005), can reduce this stiffness contrast.

### Verification of a fixed-grid finite difference numerical method

We also implemented an equally-spaced, second-order, finite difference scheme using Newton iteration, described in Appendix B. The new exact solution allows us to measure, for the first time in a rapidly-sliding marine ice sheet context, the errors from such a numerical scheme of the common type implemented in practical marine ice sheet models (e.g. Pollard and DeConto, 2009; Winkelmann and others, 2011).

Figure 9 shows that the maximum numerical thickness and velocity errors are observed to converge at much less than the optimal  $O(\Delta x^2)$  rate under grid refinement (Morton and Mayers, 2005). This is essentially because of the low regularity (loss of smoothness) of the exact solution at the grounding line. By contrast, use of the Bödvarsson (1955) exact solution in an (entirely) grounded problem, without a grounding line, confirms that the same finite difference method gives optimal  $O(\Delta x^2)$  convergence; not shown.

It is important to distinguish the errors attributable to the finite difference discretization itself from errors attributable to imperfect convergence of the nonlinear iterative solver (which is applied to solve the discretized equations). For the former type of errors we initialized the nonlinear solver with the exact solution values. These are not the exact solutions of the discretized equations but they are (obviously) close. We see converged solutions to the discretized equations down to 5 m grids. The re-

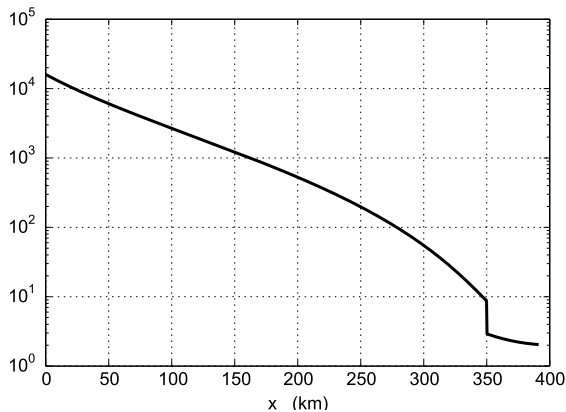


**Fig. 8.** Stiffness ratio  $|\text{Re}(\lambda_1)|/|\text{Re}(\lambda_3)|$  for the linearized problem (21), where  $\lambda_i$  are the eigenvalues of  $A(x)$  in (21).

sulting thickness and velocity errors, at the millimeter and millimeter-per-year level, respectively (Figure 9), are larger than from the adaptive (grid-free) higher-order ODE method above; compare Figure 6. Nonetheless errors at this level are certainly acceptable, if they were to represent the realistic case.

However, if we use a simple “wedge” initial iterate, which has a linear thickness profile from the upstream initial condition  $H(0)$  down to 300 m at the calving front, and a similar linear velocity profile increasing from  $u(0)$  to 300  $\text{m a}^{-1}$  at the calving front, then we see more realistic results which reflect the experience of ice sheet modelers addressing these equations. Here the initial iterate is relatively far from the exact solution. Difficulties arise in the global convergence behavior of the Newton solver, even though standard line search techniques are used in these computations (Kelley, 1987; Balay and others, 2011). For grids finer than 1 km the iteration for this scheme does not converge, apparently because the Jacobian matrix is not providing useful directional information as to the location of the solution of the discretized equations. In any case, our results suggest a lack of nonlinear solver robustness that we attribute to the nonsmooth, stiffness-constrasting properties of the problem near the grounding line.

Grounding line parameterizations (e.g. Gladstone and others, 2010; Feldmann and others, 2014) may act like homotopy continuation methods (Kelley, 1987) to improve global solver behavior in this case, but such considerations go beyond our scope. However, no regularization of grounding line discontinuities and slope discontinuities in the formulas for  $\beta(x)$  and  $h(x)$  (respectively) were applied in the current paper.

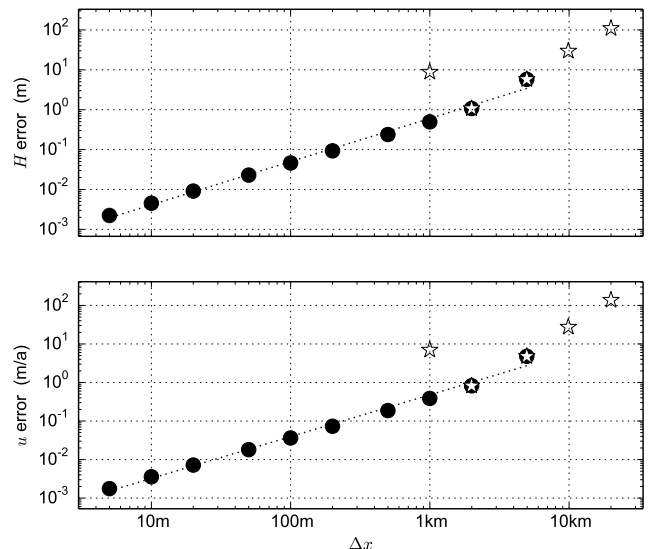


**Fig. 9.** Maximum errors in ice thickness (upper panel) and velocity (lower panel) on grids with spacing from 20 km down to 5 m. When initialized with the exact solution, the numerical scheme converges at a rate  $\Delta x^{1.08}$  for both thickness and velocity (large dots plus dotted line). For a more realistic initial iterate the convergence rate is initially good, but at resolutions below 1 km the Newton iteration fails to converge (stars; see text).

## CONCLUSION

As noted by Bueler and others (2005), Wesseling (2001), and many other sources, verification of numerical methods is a valuable first step in effective numerical modeling of realistic flows. This is especially so in geophysical flows where validation by comparison to controlled laboratory experiments is difficult. Thus the rediscovery of an exact solution to a marine ice sheet problem is a welcome development. Even though this solution is for a steady-state and flat bed case, it provides a partial alternative to hard-to-interpret intercomparison results (Pattyn and others, 2012).

Because this solution is found in some of the first work in theoretical glaciology, we have “rescued” an early approach to sliding dynamics. The “rapid-sliding” case turns out to be one of the first dynamical situations examined (Böðvarsson, 1955), even though most early efforts at global views of ice dynamics tended toward the plastic ice (Orowan, 1949; Nye, 1952), frozen bed (Vialov, 1958), and vertical-shear dominated (Weertman, 1961) models, and these came to dominate the field until recent decades.

Citations of Böðvarsson (1955) usually relate to its theory of climatic instability for glaciers and ice sheets in which surface mass balance depends on elevation. The only exception to this pattern known to the current author is that Fowler (1992) refers to the basal-shear-dominated dynamics of Böðvarsson



(1955) as “approximate results.” We hope that the current work revives interest in Böðvarsson’s ice dynamical solution and corrects (understandable) misreading of his results as approximate.

Application of the new exact solution also reveals one feature of the marine ice sheet problem that we feel has been overlooked. Namely that there is a strong stiffness contrast, in the sense of differential equations, in the flowline case at the grounding line. This is, conceptually, in addition to the loss of smoothness seen at the grounding line. Both smoothness and stiffness must be addressed by numerical methods. Modelers should have more than grid refinement in mind as they attempt to model grounding lines correctly.

### Acknowledgements (and erratum)

Comments from referees R. Gladstone and K. Hutter have focussed and improved the paper. Thanks to G. Aðalgeirsdóttir, H. Blatter, and H. Björnsson for tracking down a copy of Böðvarsson (1955) and a bibliography of the works of Gunnar Böðvarsson. Bueler and others (2005) incorrectly identify the constant accumulation SIA solution as “Bodvarsson (1955)–Vialov (1958)”. In fact it is attributable only to Vialov. Finally, note that spellings of Böðvarsson include “Bodvardsson” (e.g. in Böðvarsson (1955)) and “Bodvarsson” in the literature.

### REFERENCES

- Balay, S. and others, 2014. PETSc Users Manual, *Tech. Rep. ANL-95/11 - Revision 3.4*, Argonne National Laboratory.
- Bodvardsson, G., 1955. On the flow of ice-sheets and glaciers, *Jökull*, **5**, 1–8.
- Bueler, E. and J. Brown, 2009. Shallow shelf approximation as a “sliding law” in a thermodynamically coupled ice sheet model, *J. Geophys. Res.*, **114**, f03008, doi:10.1029/2008JF001179.
- Bueler, E., C. S. Lingle, J. A. Kallen-Brown, D. N. Covey and L. N. Bowman, 2005. Exact solutions and numerical verification for isothermal ice sheets, *J. Glaciol.*, **51**(173), 291–306.
- Feldmann, J., T. Albrecht, C. Khroulev, F. Pattyn and A. Levermann, 2014. Resolution-dependent performance of grounding line motion in a shallow model compared to a full-Stokes model according to the MISIMP3d intercomparison, *J. Glaciol.*, **60**(220), 353–360.
- Fowler, A. C., 1992. Modelling ice sheet dynamics, *Geophysical & Astrophysical Fluid Dynamics*, **63**, 29–65.
- Gladstone, R. M., A. J. Payne and S. L. Cornford, 2010. Parameterising the grounding line in flow-line ice sheet models, *The Cryosphere*, **4**, 605–619.
- Higham, D. and L. N. Trefethen, 1993. Stiffness of ODEs, *BIT*, **33**, 285–303.
- Hindmarsh, A. C., 1983. ODEPACK, A Systematized Collection of ODE Solvers, *IMACS Transactions on Scientific Computation*, **1**, 55–64, edited by Stepleman et al.
- Kelley, C. T., 1987. Solving Nonlinear Equations with Newton’s Method, *Fundamentals of Algorithms*, SIAM Press.
- Leguy, G. R., X. S. Asay-Davis and W. H. Lipscomb, 2014. Parameterization of basal hydrology near grounding lines in a one-dimensional ice sheet model, *The Cryosphere Discussions*, **8**(1), 363–419.
- MacAyeal, D. R., 1989. Large-scale ice flow over a viscous basal sediment: theory and application to ice stream B, Antarctica, *J. Geophys. Res.*, **94**(B4), 4071–4087.
- Morton, K. W. and D. F. Mayers, 2005. Numerical Solutions of Partial Differential Equations: An Introduction, Cambridge University Press, 2nd ed.
- Nye, J. F., 1952. A method of calculating the thicknesses of the ice-sheets, *Nature*, **169**(4300), 529–530.
- Orowan, E., 1949. Discussion, *J. Glaciol.*, **1**(5), 231–236.
- Pattyn, F., C. Schoof, L. Perichon and others, 2012. Results of the Marine Ice Sheet Model Intercomparison Project, MISIMP, *The Cryosphere*, **6**, 573–588.
- Pollard, David and Robert M. DeConto, 2009. Modelling West Antarctic ice sheet growth and collapse through the past five million years, *Nature*, **458**, 329–333.
- Press, W. H., S. A. Teukolsky, W. T. Vetterling and B. P. Flannery, 1992. Numerical Recipes in C: The Art of Scientific Computing, Cambridge University Press, 2nd ed.
- Schoof, C., 2005. The effect of cavitation on glacier sliding, *Proc. R. Soc. A*, **461**, 609–627.
- Schoof, C., 2006. A variational approach to ice stream flow, *J. Fluid Mech.*, **556**, 227–251.
- Schoof, C., 2007. Marine ice-sheet dynamics. Part 1. The case of rapid sliding, *J. Fluid Mech.*, **573**, 27–55.
- van der Veen, C. J., 1983. A note on the equilibrium profile of a free floating ice shelf, IMAU Report V83-15. State University Utrecht, Utrecht.
- van der Veen, C. J., 2013. Fundamentals of Glacier Dynamics, CRC Press, 2nd ed.
- Vialov, S. S., 1958. Regularities of glacial shields movement and the theory of plastic viscous flow, International Association of Scientific Hydrology Publication 47 (Symposium at Chamonix 1958—Physics of the movement of ice), 266–275.
- Weertman, J., 1961. Stability of ice-age ice sheets, *J. Geophys. Res.*, **66**, 3783–3792.
- Weis, M., R. Greve and K. Hutter, 1999. Theory of shallow ice shelves, *Continuum Mech. Thermodyn.*, **11**(1), 15–50.
- Wesseling, Pieter, 2001. Principles of Computational Fluid Dynamics, Springer-Verlag.
- Winkelmann, R., M. A. Martin, M. Haseloff, T. Albrecht, E. Bueler, C. Khroulev and A. Levermann, 2011. The Potsdam Parallel Ice Sheet Model (PISM-PIK) Part 1: Model description, *The Cryosphere*, **5**, 715–726.

### Appendix A: Böðvarsson’s little theorem

Böðvarsson (1955) does not identify a source for the exact parabolic thickness solution to his plug flow equations, and we have not been able to attribute it to earlier work. We summarize his result as the theorem that there is a unique polynomial solution  $y(x)$  to the nonlinear second-order differential equation

$$(yy')' = c_1y + c_0 \quad (\text{A1})$$

satisfying the single boundary condition  $y(0) = y_0 > 0$ , subject to both an initial downslope assumption

( $y'(0) \leq 0$ ) and to the technical inequality  $2c_1y_0 + 3c_0 \geq 0$ .

Equation (A1) is equation (17) in B  dvarsson (1955). The additional assumptions (i.e. initial downslope plus the technical inequality) are unstated, though he comments that there is “one and only one solution which is admissible from the physical point of view.”

Here we justify this little theorem and, generally following B  dvarsson (1955), derive relations among parameters which allow a solution. The unique polynomial solution to this problem may be interpreted as solving a free boundary problem for the first positive zero  $x_0 > 0$  of  $y(x)$ . In B  dvarsson’s context  $x_0 = L_0$  is the length of the glacier, the location of the margin in the “dry” case.

It is easy to see by substitution into (A1) that non-trivial solutions of degree  $d$ , i.e. of the form  $y(x) = Cx^d + (\text{lower degree})$  with  $C \neq 0$ , exist only if  $d = 2$ . In that case we seek solutions which satisfy the boundary conditions  $y(0) = y_0$  and  $y'(0) \leq 0$ , so

$$y(x) = y_0(1 - \alpha x + \gamma x^2) \quad (\text{A2})$$

for some  $\alpha \geq 0$  and  $\gamma$  which are to be determined; this is equation (18) in (B  dvarsson, 1955). Substitution of (A2) into (A1) gives the two equations

$$3y_0^2\alpha^2 = 2c_1y_0 + 3c_0 \quad \text{and} \quad 6y_0\gamma = c_1. \quad (\text{A3})$$

These two relations determine  $\alpha$  and  $\gamma$  from  $c_0$  and  $c_1$ . The first relation explains the technical inequality, noting  $3y_0^2\alpha^2 \geq 0$  of course.

In the main text, B  dvarsson’s problem relates four numbers to the unknown glacier thickness  $y(x) = H(x)$ : the initial (upstream) ice thickness  $y_0 = H_0$ , an ablation gradient  $a > 0$ , the equilibrium-line altitude  $H_{\text{ela}}$ , and a scaled sliding coefficient  $k > 0$ . He has  $c_0 = kaH_{\text{ela}}$  and  $c_1 = -ka$  in (A1) so the technical inequality says  $3H_{\text{ela}} \geq 2H_0$  after simplification. This causes the equilibrium line altitude to be relatively high on the glacier.

## Appendix B: A finite difference scheme

The steady-state equations for mass continuity (1) and stress balance (2) form a coupled system that can be approximately solved by the centered, second-order finite difference scheme described here. There is no claim that this scheme is optimal, but merely that it is a reasonable fixed-grid method for initial evaluation. Because we use it to solve a steady-state problem, it generalizes to the time-dependent case as an implicit method.

We define an equally-spaced grid on the domain  $[0, x_c]$ . Because the boundary condition at the calving front evaluates the stress  $T$ , we put the right

endpoint  $x_c$  at a “staggered” location halfway in-between grid points. Thus if  $N$  is the number of spaces then we define  $\Delta x = x_c/(N + 1/2)$  and  $x_j = j\Delta x$  for  $j = 0, \dots, N + 1$ . Denote the numerical approximations  $H_i \approx H(x_i)$  and  $u_i \approx u(x_i)$ . Let  $x_j^* = x_j + \Delta x/2$  be the staggered location, for  $j = 0, \dots, N$ . Note  $x_c = x_N^* < x_{N+1}$ . Denote  $B_j^* = B(x_j^*)$  and  $M_j^* = M(x_j^*)$ .

The mass continuity equation (1) is approximated by a second-order difference centered at the staggered location. For  $j = 0, \dots, N$ ,

$$\frac{u_{j+1}H_{j+1} - u_jH_j}{\Delta x} - M_j^* = 0 \quad (\text{A4})$$

In equation (2) we avoid infinite viscosity by using a regularization (Schoof, 2006). Let  $\epsilon = 1/x_c$  per year, i.e. a strain rate corresponding to 1 m/a velocity change over the whole domain. Also let  $q = (1 - n)/n$ , and define

$$F(u_l, u_r) = \left( \left( \frac{u_r - u_l}{\Delta x} \right)^2 + \epsilon^2 \right)^{q/2} \frac{u_r - u_l}{\Delta x}. \quad (\text{A5})$$

Then we approximate the stress  $T$  at staggered points,

$$T_j^* = B_j^* (H_j + H_{j+1}) F(u_j, u_{j+1}), \quad (\text{A6})$$

for  $j = 0, \dots, N$ . Equation (2) is approximated by

$$\frac{T_j^* - T_{j-1}^*}{\Delta x} - \beta_j u_j - \rho g H_j \frac{h_{j+1} - h_{j-1}}{2\Delta x} = 0 \quad (\text{A7})$$

for  $j = 1, \dots, N$ , where  $\beta_j = k\rho g H_j$  if the ice is grounded at  $x_j$  (i.e. if  $\rho H_j \geq \rho_w(z_o - b)$ ) and  $\beta_j = 0$  if the ice is floating, and where  $h_j = H_j + b$  if the ice is grounded and  $h_j = \omega H_j + z_o$  if the ice is floating. Thus equation (A7) applies as stated both for grounded and floating ice.

At this point we have  $2N + 4$  scalar unknowns, namely  $u_j$  and  $H_j$  for  $j = 0, \dots, N + 1$ . There are  $2N + 1$  nonlinear equations in (A4) and (A7) above. The two upstream Dirichlet equations (6), namely  $u_0 = u(0)$  and  $H_0 = H(0)$ , brings the number of equations to  $2N + 3$ . The following approximation of the calving front condition (7), completes the system:

$$\frac{1}{2}\omega\rho g \left( \frac{H_N + H_{N+1}}{2} \right)^2 = T_N^*, \quad (\text{A8})$$

where  $T_N^*$  is the approximation given in (A6).

Thus we have a system of  $2N + 4$  nonlinear equations in the same number of unknowns. One can write this system abstractly as  $\mathbf{F}(\mathbf{v}) = 0$ . These equations are solved by Newton’s method (Kelley, 1987), as implemented in the PETSc library (Balay and others, 2011). A residual evaluation function computes  $\mathbf{F}(\mathbf{v})$  given  $\mathbf{v}$ . A finite-difference Jacobian matrix  $J = \mathbf{F}'$  can then be computed by PETSc,

and this allows us to solve systems up to size about  $N = 10^3$ . We also implemented an exact Jacobian using by-hand differentiation of the above formulas. For initial guesses sufficiently near the exact solution, this exact Jacobian permits solutions of the system for up to  $N = 10^5$ . A full analysis of the robustness and convergence rate of this Newton solver is beyond the scope of the current paper.